Commun. Theor. Phys. **63** (2015) 77–85 Vol. 63, No. 1, January 1, 2015

An Exotic Phase Change in Dynamic Electrorheological Fluids*

Tang Qiang-Guo (唐强果),[1] HUANG Jun-Ying (黄俊樱),[1] LI Cong (李丛),[2] ZHENG Jie (郑杰),[1]
MENG Xian-Wen (孟现文),[1] HUANG Ji-Ping (黄吉平),[1,†] and ZHOU Lu-Wei (周鲁卫)[1,‡]

[1]Department of Physics and State Key Laboratory of Surface Physics, Fudan University, Shanghai 200433, China

[2]College of Information Technology, Shanghai Ocean University, Shanghai 201306, China

(Received September 23, 2014; revised manuscript received September 29, 2014)

Abstract *It is well known that constant or time-varying electric fields can induce phase changes in electrorheological (ER) fluids, from a liquid to semi-solid state, provided the field strength is larger than some critical value. We describe here an experimental and theoretical study considering yet a different class of phase changes, specifically those for an ER fluid in the presence of both shear flow and a time-varying electric field. We note that as the frequency of the field is decreased, the ER fluid will go from a liquid to an intermediate transition state, and eventually to a shear banding state. Our theoretical analysis further indicates that this phase change originates from competing effects of viscous and electrical forces. Ultimately, we conclude that it is possible to achieve various states and corresponding (desired) macroscopic properties of dynamic colloidal suspensions by adjusting the frequency of the externally applied electric field.*

PACS numbers: 41.20.Cv, 02.40.-k
Key words: electrorheological (ER) fluids, electric field, transition state

1 Introduction

An electrorheological (ER) fluid can change from a liquid to semi-solid state within milliseconds when the fluid is subjected to an external applied electric field generated by direct current (DC) or alternating current (AC) voltage. This process is known to be reversible.[1−4] The mechanical properties of ER fluids have attracted much research interest, particularly after giant ER or polar molecules-modified ER (PMER) fluids were invented.[2−3,5−14] Moreover, Calandra *et al.* found such electrorheological effects at very low applied fields (≈ 400 V/mm) in systems where a (carefully chosen) solvent, via certain solvent-nanoparticle interactions, acted as both a dispersing medium and a nanoparticle capping agent.[15] This finding paved the way for many new applications of ER fluids exposed to very low electric fields. On the other hand, since most ER fluids are employed in dynamic states under a variety of shear flow conditions, increasingly we see studies of such flow state of ER fluids, so-called electrohydrodynamic effects.[16−18] Electrohydrodynamics considers both the effect of fluid motion on the field, as well as the influence of field on the fluid motion. Melcher and Taylor investigated the role of interfacial shear stress in determining properties of various ER fluids.[16] Roberts *et al.* examined the instabilities of AC electrohydrodynamic ER fluids in thin liquid films, using lubrication theory to exert control over the size and shape of the surface pillars.[17] Khusid *et al.* studied the mechanism of interfacial polarization of the particles and how it affects DC electric-field-induced aggregation. Their results show that the thermodynamic properties of such suspensions are strongly influenced by certain dielectric relaxation effects.[18] Also, lamellar structures were observed in the plate-plate geometry.[19−21] The higher the applied field strength (or the lower the rotating speed), the greater the number of layer rings.[19] Klingenberg *et al.* discovered that the liquid layers attached to the electrodes become thinner in the presence of DC electric fields when the shear rate is increased.[22] The work of Volkova *et al.* verified that a nematic-to-isotropic transition in ER fluids can further affect shear stresses.[23] By using a two-phase dipole fluid model,[24−25] our recent computer simulation study produced lamellar structures and shear banding in a disk-disk geometry using a DC electric field.[26] Recently, the study of self-assembled tunable networks of polymer fibres under an AC electric field shows that the frequency and amplitude of the electric field affect the morphology and relative length of polymer fibres.[27]

In this study, we use a microscope-attached electrorheometer to investigate the dynamic properties of 1,4-butyrolactone-TiO_2 ER fluids[28] exposed to an AC electric field. The electric field between the inner rotator and outer stator is maintained at 700 V/mm. In this way, the electric interaction forces between particles can be

*Supported by the National Natural Science Foundation of China under Grant Nos. 10334020, 10974030, 10574027, 11222544, the Fok Ying Tung Education Foundation under Grant No. 131008, and the Program for New Century Excellent Talents in University (NCET-12-0121), the CNKBRSF under Grant No. 2011CB922004

†E-mail: jphuang@fudan.edu.cn
‡E-mail: lwzhou@fudan.edu.cn

changed by adjusting the field frequency.[29−32] Lan *et al.* studied the frequency dependence of the ER response in a suspension of barium titanate spherical particles suspending in silicone oil.[29] Subjected to such sinusoidal electric fields, the shear stresses increased sharply with frequency below 500 Hz, and quickly reached a saturation value. This phenomena can be explained using permittivity mismatch theory. Wen *et al.* studied the ER fluid consisting of glass spheres and silicone oil and found that with increasing frequency of the externally applied electric field, the shear stress decreased below 1000 Hz and finally reached a stable value.[3] By using calculations from first-principles, their theory has good quantitative agreement with other's experimental results.[33]

We observe yet a different class of phase changes in the ER fluid in the presence of both shear flow and AC electric field. When the frequency of the AC field is decreased, we observe that the ER fluid changes from a liquid state, to a transition state, and eventually to a shear banding state. It will be shown that this phase change originates from competing effects of electric and viscous forces.

2 Experiment

The sample used in this experiment is a colloidal suspension of silicone oil and 1,4-butyrolactone modified TiO_2 powder. The viscosity of silicone oil is 20 cSt at room temperature. The volume fraction of 1,4-butyrolactone modified TiO_2 powder is 0.43 with sedimentation ratio above 99% after 500 hours of testing.[28] The 1, 4-butyrolactone modified TiO_2 powder is synthesized with the sol-gel method. The average radius of suspended particles is 460 nm. The colloidal suspension consisting of such particles has a significant response to externally applied electric fields. The quasi-static yield stress of the PMER fluid, which is Newtonian under zero electric field, reaches 48.1 kPa at 5 kV/mm.[28]

The apparatus consists mainly of three parts: an AC high voltage generator, a Haake–Mars II electrorheometer and a lens system with a charge-coupled device (CCD) camera. The AC high-voltage generator can output up to 1 kV of sinusoidal waveforms with frequencies ranging from 6 Hz to 1 kHz. The AC voltage generating system contains of three parts: a voltage signal generator, a custom-made power amplifier and transformer pair. One transformer is made of silicon sheets and is designed for frequencies below 500 Hz; the other made using a ferrite core and is designed for frequencies above 500 Hz. Each transformer is immersed in a transformer oil tank to maintain electrical stability. During the experiment, the voltage of the AC high voltage generator was monitored to keep the output voltage stable. The Haake–Mars II electrorheometer is used to shear the ER fluid at a constant apparent shear rate and to measure the shear stress with an error less than 0.01 Pa. The CCD camera (JAI Ltd., Japan) and corresponding lens system is used to acquire top views of the dynamic features of the particles, using 1.5 million pixels per frame, at 30 frames per second.

To reset conditions to a neutral state, each new experiment begins by shearing the ER fluid without external fields for 5 minutes. After applying an external electric field, the shear stress is acquired by electrorheometer. Meanwhile, the top view of liquid-air interface is taken by the CCD camera in the microscope. Due to the low transparency of ER fluids, it is difficult to observe the particle movement inside the fluids. Our simulations with finite element analysis show that the surface flow properties are the same as that inside (see below for details). The shear stress and particle speed profiles become stable after several minutes and then the data and pictures are recorded for further study. Wall slip is not observed in rheological measurements with increasing frequency. Figure 1(b) shows how to measure the velocity of a particle cluster based on the horizontal interface of the fluid. The CCD camera records positions of particles every 1/30 s. The velocity of a particle cluster between two frames is calculated by using the Euclidean distance. This algorithm holds true in the limit of a large cylinder radius, or a small distance between particles, and it is true in this study. The travel distance of a particle measured every two frames is smaller than 0.4 mm, which is about 2% of the diameter of the inner cylinder (20 mm).

3 Results

First, we determine profiles of ER particle speeds versus particle distances to the stator, r, for different frequencies of the applied AC electric field. The stator is at $r = 0$, while the rotor is at $r = 1$ mm, as indicated in Fig. 1. The slope of the particle speed profile is equal to the apparent shear rate. According to the experimental results shown in Fig. 2, when the field frequency is 600 Hz [Fig. 2(b)], the profile of particle speed versus distance to the stator is nearly linear. The ER fluid behaves as a liquid with a low shear stress of 27.1 Pa, and it is considered to remain in a liquid state at this frequency.

When the frequency of the applied field is 50 Hz and the shear stress is 99.7 Pa [Fig. 2(e)], the slope of the particle speed profile is near zero when the distance to the rotor is below 0.1 mm, and then increases gradually with the distance when the distance is above 0.1 mm. In the jammed area, the fluid behaves like a solid, while in the flowing area, like a liquid. There is not a sharp change of the the particle speed profile slope at the interface between flowing and jammed areas. This particular phenomenon is not a shear banding state, but rather a transition state. At the field frequency of 15 Hz [Fig. 2(i)], the shear stress is larger than those at the field frequencies of 50 and 200 Hz, and the slope of the particle speed profile is almost zero when r is less than 0.4 mm. The particle speed increases abruptly when r is larger than 0.4 mm with a constant slope. This is also a coexistence state of liquid and solid that is found at a field frequency of 50 Hz. However, in contrast to the case at 50 Hz where the profile slope is continuous, the slope (namely, the local shear rate) for 15 Hz at the interface between flowing and jammed areas

shows an abrupt change, which is clearly a shear banding phenomenon.[34] Therefore this state is called a shear banding state. We thus observed a dynamic transitions process of the ER fluid: starting from a liquid state, then a transition state – coexistence of flowing and jammed structures without a distinct boundary between the two structures, and finally a shear banding state – coexistence of flowing and jammed structures with well-established boundary between the two structures.

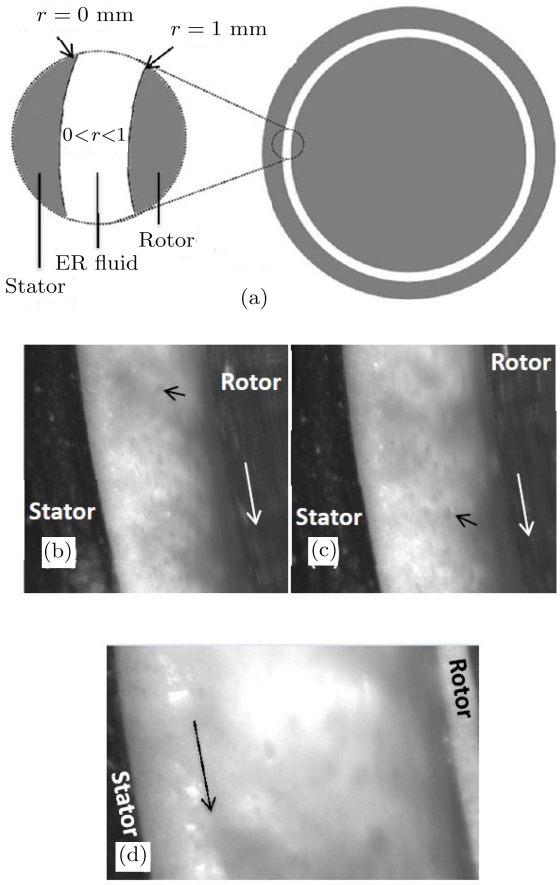

Fig. 1 (Color online) (a) Two-dimensional schematic graph of the electrorheometer with a microscopic CCD that measures rheological properties of ER fluids and takes images of the particle structure of colloidal suspensions. The rotor (inner cylinder) with radius of 10.35 mm rotates (as shown by the white arrow in (b) or (c)) at a speed of 4 RPM with a shear rate of 4.14 s^{-1}, while the stator is fixed. Two coaxial cylinders with the gap of 1 mm and the height of 55 mm are constructed. $r = 0$ mm (or 1 mm) denotes the edge of the stator (or rotor). $0 < r < 1$ mm denotes the gap between the stator and rotor that is filled with the model ER fluid. (b) and (c) show the movement of a particle cluster (pointed by a black arrow in each panel) in the gap between the stator and rotor. The rotation direction of the rotor is indicated by the white arrow. (c) is about 0.17 s later than (b). (d) is the CCD picture of a shear banding state. The black arrow in (d) points the boundary of jammed (left) and flow (right) areas.

Yoshimura *et al.* have proposed a parameter, φ_ω (= $\omega_E R_1 \tau$) to describe slippage of materials on the surface of rotator or stator in concentric cylinder measurements, where R_1 is the stator radius in a concentric-cylinder geometry, and the emulsion rotates around the stator with angular velocity ω_E.[35] They suggest that the nature of the plot of rotational speed divided by stress vs. stress is similar to that of φ_ω vs τ. The abbreviation of "rounds per minute", RPM, represents the angular velocity of the rotator, and RPM/τ is proportional to the reversed viscosity. Thus the curve of RPM/$\tau - \tau$ provides qualitative information about the flow behavior of the slip layers. RPM/τ should be linear with shear stress given the absence of boundary slip. Their results show that there exists boundary slip in concentric-cylinder geometry. In our experiments, the boundary slip is not evident under the condition of angular velocities of rotator of 4 RPM, and there exists shear banding throughout the depth. We have measured rheological properties of the PMER fluid to assess the boundary slip using Yoshimura *et al.*'s method. In Fig. 3, panels (a) and (b) give the rheological curves of the PMER fluid at electric field frequencies of 6, 15, 25, 35, 45, 50, 80 and 200 Hz, and applied electric field of 700 V/mm. The PMER fluid consists of 3 g PMER powders per 2.2 ml silicone oil. Panels (c) and (d) plot RPM/$\tau - \tau$ at the same field frequencies with arrows indicating the deviation from the linear section of the curves due to wall slip. RPM/τ is about 0.02 at 4 RPM in the linear region of the curves, where no obvious wall slip is evident. Yoshimura *et al.*'s method suggests that the boundary slip is very small and can be ignored at and below 4 RPM. As mentioned above, the shear banding experiments are conducted when the rotational speed of the rotator is about 4 RPM. The shear banding throughout this region is the main factor that restricts slip at the boundary under low rotational speed.

Owing to the high concentration of the ER fluid, images observed in this work only reflect the behavior at the liquid-air interface of the ER fluid. It is therefore important to also mention the effects of the electric field on the liquid-air interface. The electric field within the liquid region is not uniform, however is not expected to affect our qualitative results (both experimental and theoretical). For our experiment, the frequencies of interest are less than 1 kHz. Thus, the quasi-static approximation can be adopted to model the effect of electric field. In this regard, at the interface between the ER fluid and air, if the strength of electric field on the air side is E_a, the strength of equivalent electric field within the ER fluid side could be $E_{\rm ER} = E_a/\epsilon_{\rm ER}$ due to the boundary condition of electric displacement, where the effective dielectric constant of ER fluids is denoted by $\epsilon_{\rm ER}$. Here we have assumed E_a is normally incident onto the interface, thus yielding the maximum difference of $E_a - E_{\rm ER}$. In other words, the strength of electric field within the ER fluid side should generally be between $E_{\rm ER}$ and E_a (which corresponds to the case where the electric field, E_a, is almost parallel to the interface).

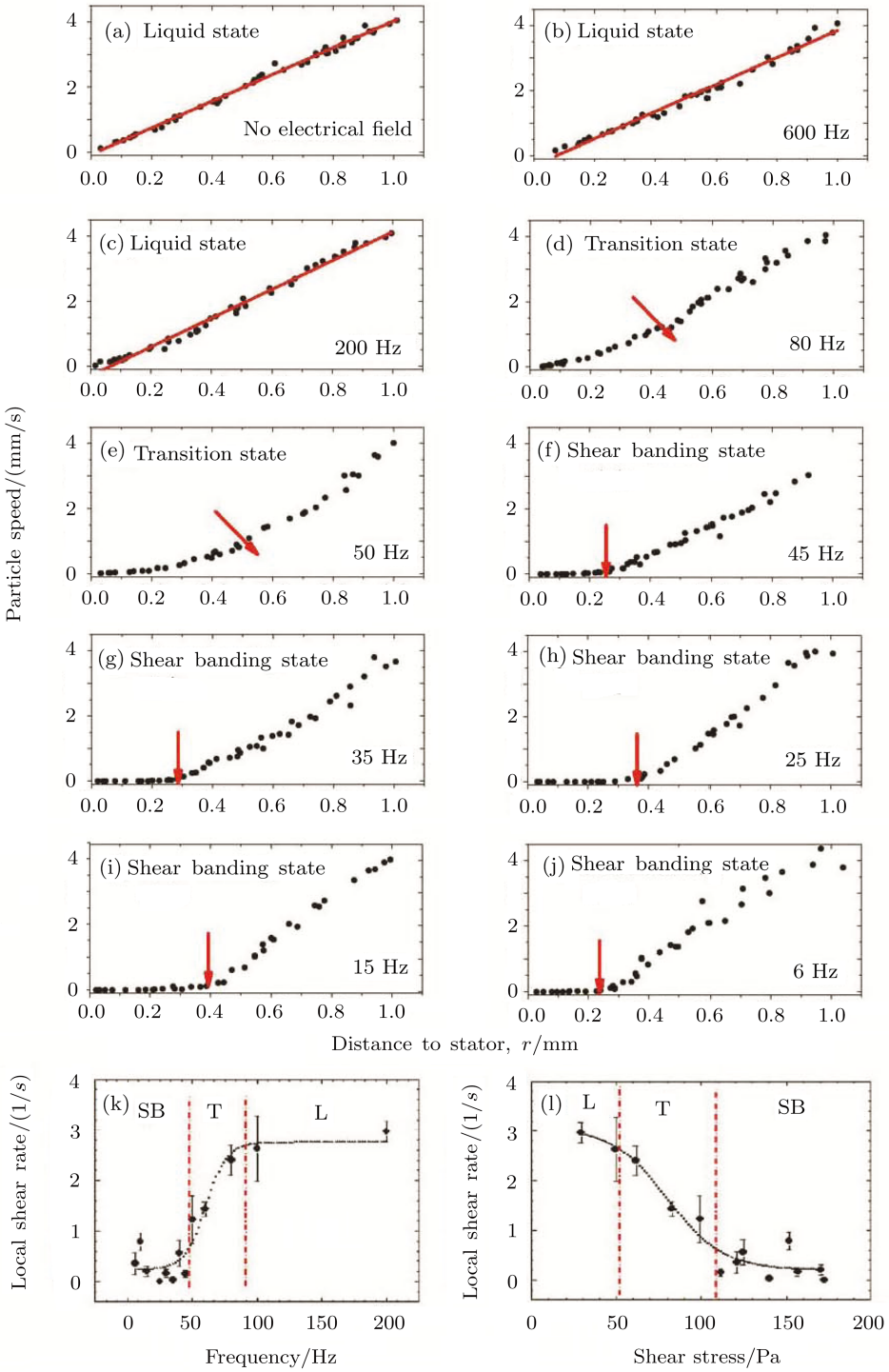

Fig. 2 (Color online) Profiles of particle speeds versus the distance to the stator, r (as indicated in Fig. 1(a)). The edge of stator is at $r = 0$ mm, and that of rotor, $r = 1$ mm. (a) shows the case of zero electric field (shear stress: 25.4 Pa); for (b)–(j), the intensity of the applied electric field is 700 V/mm. The field frequencies are (b) 600 Hz (shear stress: 27.1 Pa), (c) 200 Hz (shear stress: 29.2 Pa), (d) 80 Hz (shear stress: 61.6 Pa), (e) 50 Hz (shear stress: 99.7 Pa), (f) 45 Hz (shear stress: 111.5 Pa), (g) 35 Hz (shear stress: 139.8 Pa), (h) 25 Hz (shear stress: 172.4 Pa), (i) 15 Hz (shear stress: 170.6 Pa), and (j) 6 Hz (shear stress: 120.8 Pa). (a)–(c) the liquid state, (d)–(e) the transition state, and (f)–(j) the shear banding state. The corresponding slopes (shear rates) of liquid state are (a) 4.11 s^{-1}, (b) 4.16 s^{-1} and (c) 4.42 s^{-1} . Red arrows are added to highlight the greatest change zone of speed profiles. (k) Dependence of local shear rates near the stator on the frequency of the applied electric field. (l) Local shear rate near the stator versus shear stress. Each point in (l) corresponds to the point in (k) with the same local shear rate and frequency value. The dotted curves show the trends of shear rates versus (k) frequencies or (l) shear stresses in the area near the stator. "SB", "T" and "L" stand for shear banding, transition and liquid states, respectively, divided by two vertical dot-dashed lines.

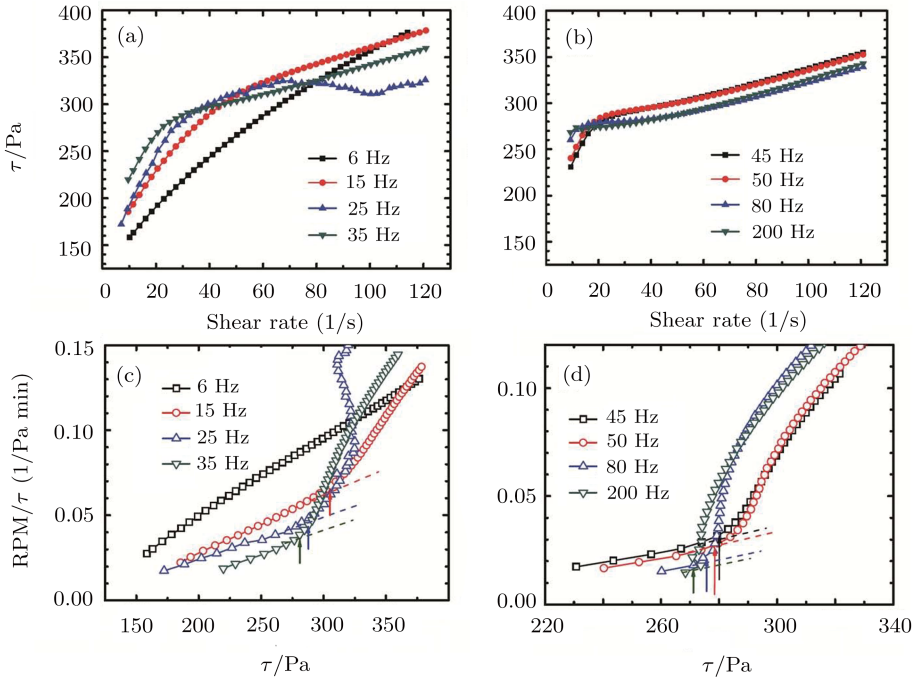

Fig. 3 (Color online) Assessments of boundary slip in a concentric cylinder measurement of rheological properties of the PMER fluid. Panels (a) and (b) give the rheological curves of the PMER fluid at electric field frequencies of 6, 15, 25, 35, 45, 50, 80, and 200 Hz. Panels (c) and (d) plot RPM/$\tau - \tau$ at the same field frequencies. The arrows indicate the deviation from the linear section of the curves due to wall slip. The applied electric field is 700 V/mm, and the PMER fluid consists of 3 g PMER powders per 2.2 ml silicone oil.

Because of the low transparency of ER fluids, it is difficult to observe the particle movement inside of the fluids. According to the experiments, we have done simulations with the finite element analysis using COMSOL MultiPhysics (a commercial software). Without much loss of generality, we construct a three-dimensional simulation cell formed by two coaxial cylinders with a gap of 1 mm and a height of 11 mm. The inner coaxial cylinder has a radius of 10.35 mm and a height of 10 mm, and the outer cylinder has a radius of 11.35 mm and a height of 11 mm. The simulation is based on the Onsager principle of least dissipation, which refers to the rules governing the optimal paths of deviation from and to restoration to equilibrium.[24,36] The consistent mathematical scheme is solved with the four coupled physical fields:[26] two incompressible Navier–Stokes fluids (one for the oil phase and the other for the particle phase), one convection-diffusion physical field for continuity equations of ER particles, and the external electric field.

The coupled equations of motion for the solid particles phase (indicated by subscript "p") and fluid oil phase (indicated by subscript "f") are given by[19,26,37]

$$\rho_p\Big(\frac{\partial \vec{V}_p}{\partial t} + \vec{V}_p\cdot \bigtriangledown \vec{V}_p\Big) = -\bigtriangledown p_p + \bigtriangledown\cdot\tau^p_{\rm visc} + n'\bigtriangledown\mu + K(\vec{V}_f - \vec{V}_p)\,, \quad (1)$$

$$\rho_f\Big(\frac{\partial \vec{V}_f}{\partial t} + \vec{V}_f\cdot \bigtriangledown \vec{V}_f\Big) = -\bigtriangledown p_f + \bigtriangledown\cdot\tau^f_{\rm visc} + K(\vec{V}_p - \vec{V}_f)\,, \quad (2)$$

$$\dot{n}' + \vec{\bigtriangledown}\cdot\vec{J} = \partial_t n + \vec{V}_p\cdot\vec{\bigtriangledown}n' + \vec{\bigtriangledown}\cdot\vec{J} = 0\,, \quad (3)$$

with the supplementary incompressibility conditions $\bigtriangledown\cdot\vec{V}_{s,f} = 0$. $\bigtriangledown\cdot\tau_s = n\bigtriangledown\mu$ is the volume force induced by the electric field and neighboring dipoles, and n is the number density of ER particles. The left-hand side of Eq. (1) is the time change rate of the particle momentum consisting of the local and the convective accelerations, and is equal to the sum of the surface forces per unit volume, including three terms on the right-hand side of Eq. (1). The first term is the particle pressure force, the second and the fourth terms represent viscous forces, and the third one is the body force per unit volume caused by the electric field. Equation (2) is an equation for the fluid, and it contains all the terms for particles except for the body force per unit volume caused by electric field. Equation (3) is the continuity equation for n, the local number density of particles.

These three equations, together with the non-slip boundary conditions, form a suitable mathematical scheme for analysis. The simulation is conducted with the following parameters: the dielectric constants of fluid and particles are respectively 2.5 and 38, the viscosity of fluid is 20 cSt, the radius and mass of an ER particle is 460 nm and 1.2×10^{-15} g, and the density of fluid is $\rho_f = 0.96$ g/m^3.

Simulation results show that the flow properties inside the sample cell appear to be the same as the ones on the surface; see Fig. 4. Under the external field and shearing flow, there exist not only a radial shear band (such as in Fig. 1(d)), but also an axial shear band throughout the depth.[19] Because of the existence of the axial shear band, the structure of shear banding varies throughout the depth while maintaining the principal features of the particle speed profile on horizontal layers. It is clear that shear bands occur not only at the surface of ER fluids ($H = 11$ mm), but also inside the ER fluid when the rotating speed of the rotor is 4 RPM, the volume fraction is 0.43, and the external DC electric field is 700 kV/mm. When the ER fluids with the high solid-state volume fraction under external electric fields are sheared, the energy of ER particles can not dissipate fast through the oil. The energy can dissipate only by the friction among ER particles timely, thus causing the speed difference of ER particles inside and on the surface of the suspension. Finally, the results obtained from the speed curves are also affected by the fluctuation of the solid particles phase in motion.

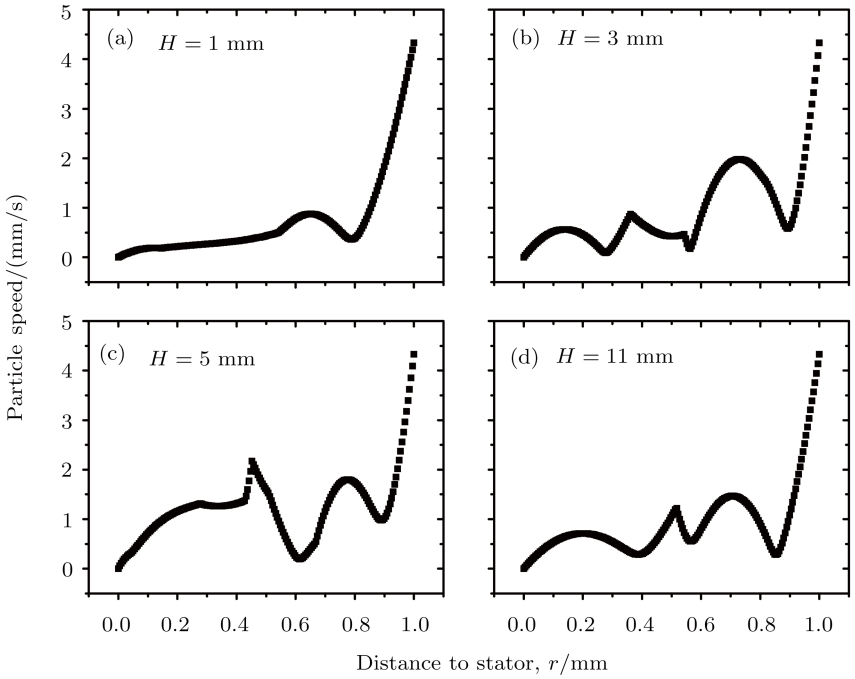

Fig. 4 Three-dimensional simulation results with the finite element analysis under a similar condition to that in the experiments. Profiles of particle speeds on horizontal layers versus the distance to the stator with an external DC electric field of 700 V/mm. The edge of stator is at $r = 0$ mm, and that of rotor, $r = 1$ mm. The simulation cell constitutes of two coaxial cylinders with the gap of 1 mm and the height of 11 mm. H represents the height of the point being observed in the suspension from the bottom of the gap. The rotating speed of the rotor is 4 RPM. The volume fraction is 0.43.

We have proposed[38] that the structure criterion for the shear banding is $S(r) = |f_e(r)|/|f_h(r)| > 1$, where $f_e(r)$ is the jamming stress due to electric interaction and $f_h(r)$ is the fluidizing stress due to hydrodynamic interaction. Namely, $S(r) > 1$ is the criterion of jamming structure in the shear banding phase; while $S(r) < 1$, $f_h(r)$ surpasses $f_e(r)$, the banding structures are destroyed gradually, and the whole suspension is eventually fluidized completely without any shear banding.

According to the previous discussion, at the transition and the shear banding states, the local shear rate is different from the apparent shear rate. Figure 2(k) shows the relation between local shear rates near the stator and field frequencies. Below 50 Hz, the shear rate near the stator is close to zero. The shear rate near the stator increases quickly with frequency up to about 100 Hz, beyond which the shear rate near the stator is relatively stable. We have already established that when the profile is linear, this state is identified as a liquid state. The state without an abrupt change of particle speed slope at the interface between flowing and jammed areas is identified as a transition state. Otherwise, a shear banding state appears. Based on this understanding, particle speed profiles under different frequencies are examined, and the result is shown in Fig. 2(l). When the shear stress is less than 55 Pa, the curve of particle speeds versus the distance to the stator is almost linear, therefore the ER fluid stays at the liquid state. In this state, the local shear rate is nearly steady within the measurement error. When the shear stress

is within a range between 55 Pa and 105 Pa, the curve changes gradually without an abrupt slope change. This corresponds to the transition state. It is clear to see that the shear rate of jammed areas decreases quickly while the shear stress increases. When the shear stress is larger than 105 Pa, the profile of particle speeds versus the distance shows an abrupt change in the slope [Fig. 2(f)]. Then the ER fluid stays at a shear banding state. In this case, the shear rate near the stator is almost zero while that near the rotor increases with shear stresses. This means the size of the flowing area is reduced. Above all, the ER fluid experiences three states when the field frequency changes from 6 to 200 Hz. For ER fluids in a disk-disk condition under a DC field, it is shown that the denser rings (a shear banding phenomenon) correspond to the larger shear stress. Also, when the intensity of the external electric field increases, the number of rings increases.[21] In this work, an exotic phase change has been observed when the frequency of the external electric field changes. However, in order to further understand the above experimental findings, further theoretical analysis is provided below.

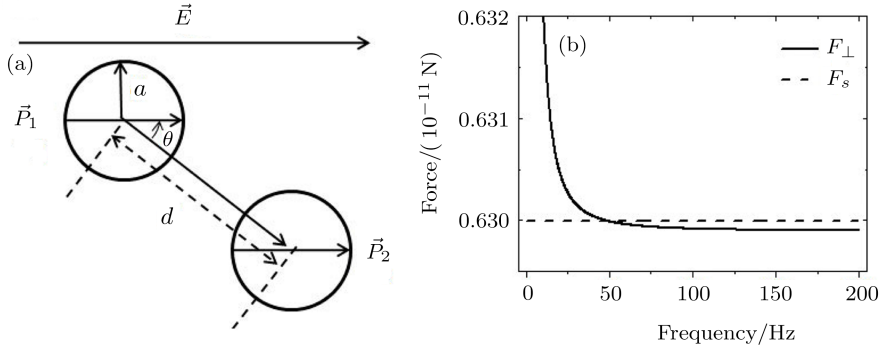

Fig. 5 (a) Sketch of two close spherical particles in the presence of an external electric field, E. Either P_1 or P_2 is the induced dipole moment of the corresponding particle, a is the radius of particle, d is the distance between the centers of two particles, and θ is the angle between $\vec{E}$ and the center-to-center line of the two particles. (b) Comparison between $F_\perp$ and F_s. Parameters adopted from the experiment: $\varepsilon_f = 2.5$, $\sigma_f = 2.5 \times 10^{-11}$ S/m, $\varepsilon_p = 38$, $\sigma_p = 2.2 \times 10^{-9}$ S/m, $E = 700$ V/mm, and $a = 460$ nm. Other parameters taken for the calculations: $d/a = 2.08$, $\theta = 36^\circ$, and $v = 1.99 \times 10^{-2}$ mm/s.

4 Theoretical Analysis

In the absence of an externally applied electric (or other) field, ER particles will be uniformly dispersed in silicone oil. In the presence of an electric field, particles become polarized and there results an electric interaction force between particles.[31,39–40] The complex dielectric permittivity of particles is $\tilde{\varepsilon}_p(\omega) = \varepsilon_p\varepsilon_0 + \sigma_p/\mathrm{i}\omega$, while that of silicone oil is $\tilde{\varepsilon}_f(\omega) = \varepsilon_f\varepsilon_0 + \sigma_f/\mathrm{i}\omega$. Here ε_0 is the permittivity of free space; σ_p and σ_f are the conductivity of particles and silicone oil, respectively; ε_p and ε_f are the relative permittivity of particles and silicone oil, respectively; ω is the angular frequency of the external AC electric field directed along x axis; and $\mathrm{i} = \sqrt{-1}$. It is difficult to quantitatively understand the above experimental results since the structure of system is difficult to model in detail. However, we could be able to qualitatively understand the experimental results obtained above by considering the electric interaction force between two close spherical particles with a radius of a[40–42] suspended in the ER fluid; see Fig. 5(a).

Let us start by considering the two boundary conditions for electric potentials, $\tilde{\varphi}_p$ (for a particle) and $\tilde{\varphi}_f$ (for the oil):

$$\tilde{\varphi}_p = \tilde{\varphi}_f \,, \tag{4}$$

$$\tilde{\varepsilon}_p \frac{\partial\tilde{\varphi}_p}{\partial x} = \tilde{\varepsilon}_f \frac{\partial\tilde{\varphi}_f}{\partial x} \,. \tag{5}$$

Then, the solution of Laplace's equation,

$$\nabla^2\tilde{\varphi} = 0 \,, \tag{6}$$

yields the induced dipole moments, $\tilde{P}_1$ and $\tilde{P}_2$, of the two spherical particles,

$$\tilde{P}_1 = \tilde{P}_2 = 4\pi\varepsilon_f\varepsilon_0 \frac{\tilde{\varepsilon}_p - \tilde{\varepsilon}_f}{\tilde{\varepsilon}_p + 2\tilde{\varepsilon}_f} a^3 E_f \,.$$

Here E_f is the local electric field in the oil. To take into account the many-body (local field) effect, we use the effective complex dielectric permittivity of the system, $\tilde{\varepsilon}_{\mathrm{eff}}$ (here $\tilde{\varepsilon}_{\mathrm{eff}}(\omega) \equiv \varepsilon_{\mathrm{eff}}\varepsilon_0 + \sigma_{\mathrm{eff}}/i\omega$; note $\varepsilon_{\mathrm{eff}}$ and σ_{eff} are both real), to replace $\tilde{\varepsilon}_f$ in the above equation. As a result, we obtain

$$\tilde{P}_1 = \tilde{P}_2 = 4\pi\varepsilon_{\mathrm{eff}}\varepsilon_0 \frac{\tilde{\varepsilon}_p - \tilde{\varepsilon}_{\mathrm{eff}}}{\tilde{\varepsilon}_p + 2\tilde{\varepsilon}_{\mathrm{eff}}} a^3 E \,, \tag{7}$$

where E is the external electric field according to the definition of effective medium.[43] Owing to the effective medium approximation,[43–44] which includes many-body (local-field) effects, $\tilde{\varepsilon}_{\mathrm{eff}}$ is given by the following equation,

$$p\frac{\tilde{\varepsilon}_p - \tilde{\varepsilon}_{\mathrm{eff}}}{\tilde{\varepsilon}_p + 2\tilde{\varepsilon}_{\mathrm{eff}}} + (1-p)\frac{\tilde{\varepsilon}_f - \tilde{\varepsilon}_{\mathrm{eff}}}{\tilde{\varepsilon}_f + 2\tilde{\varepsilon}_{\mathrm{eff}}} = 0 \,, \tag{8}$$

where p is the volume fraction of 1,4-butyrolactone modified TiO_2 particles ($p = 0.43$ in this work). It is worth

noting that Eq. (8) holds for symmetrical structure.

In the absence of an external shear field, the line connecting the centers of the two ER particles is directed along the direction of the external electric field. However, in the presence of a shear field, this line deviates from this direction. The electric interaction force between the two spheres suspended in the many-particle system, F_e, is given by $F_e = ||F'^*| - |F^*||$, where F^* (or F'^*) is the interparticle force between the two spherical particles for the transverse (or longitudinal) field case according to the many-body dipole-induced dipole model:[40]

$$F^* = -4\pi\varepsilon_{\rm eff}\varepsilon_0(E\sin\theta)^2a^3b\sum_{n=0}^{\infty}(-b)^n\Phi_n\,, \tag{9}$$

$$F'^* = -4\pi\varepsilon_{\rm eff}\varepsilon_0(E\cos\theta)^2a^3b\sum_{n=0}^{\infty}(2b)^n\Phi_n\,. \tag{10}$$

Here,

$$b=\frac{\tilde{\varepsilon}_p-\tilde{\varepsilon}_{\rm eff}}{\tilde{\varepsilon}_p+2\tilde{\varepsilon}_{\rm eff}}\,,\quad \Phi_n=\frac{\sinh\alpha\cosh\alpha\sinh^2[(n+1)\alpha]-(n+1)\sinh^2[\alpha]\cosh[(n+1)\alpha]}{(2a/3)\sinh^4[(n+1)\alpha]}\,,\quad \cosh\alpha=\frac{d}{a}\,,$$

d is the distance between the centers of the two particles [Fig. 5(a)], and θ is the angle between the field direction and the line connecting the centers of the two spheres [Fig. 5(a)]. In the above two equations, we have taken into account both local-field effects of the many-particle system (according to Eq. (8)) and multipolar interactions between the two spherical particles. It is worth remarking that the multipolar interactions only include the dipole-induced dipole interaction.[40]

On the other hand, the electric interaction force between the two spheres, F_e, possesses a component perpendicular to the direction of external electric field, which is denoted by $F_\perp$,

$$|F_\perp| = F_e\sin\theta\,. \tag{11}$$

Similarly, the component parallel to the direction of the external electric field, $F_{||}$, is given by

$$|F_{||}| = F_e\cos\theta\,. \tag{12}$$

While the viscous (Stokes) force, F_s, induced by shearing is a force destructing the static structure of the two almost touching particles in the ER fluid, $F_\perp$ tends to sustain this static structure. As a result, the competition between $F_\perp$ and F_s can be used to account for the flowing phases as revealed above. The viscous force, F_s, acted upon one of the two particles can be approximately given by

$$F_s = 6\pi\eta_{\rm eff}av\,, \tag{13}$$

with $v = v_p - v_f$. Here, v_p (or v_f) is the velocity of the particle and silicone oil, and $\eta_{\rm eff}$ is the effective viscosity of the system. To take into account the many-body effects, we use the following equation to determine $\eta_{\rm eff}$,[45]

$$\frac{\eta_{\rm eff}-\eta_f}{\eta_{\rm eff}+(3/2)\eta_f} = p\frac{\eta_p-\eta_f}{\eta_p+(3/2)\eta_f}\,, \tag{14}$$

where η_f is the viscosity of silicone oil ($\eta_f = 20$ cSt) and η_p is the viscosity of 1, 4-butyrolactone modified TiO_2 particles ($\eta_p \to \infty$).

As shown in Fig. 5(b), $F_\perp$ decreases as frequencies increase. For a low frequency (say, ≤ 45 Hz), the electric interaction force between particles ($F_\perp$) is much stronger than the viscous force (F_s). Therefore, the particles near the stator may not flow due to the relatively large $F_\perp$, or alternatively due to the relatively weak F_s originating from a small velocity difference, v. In contrast, particles located at the region near the rotator have a larger velocity difference, v, and hence F_s can be much larger than $F_\perp$. As a result, particles near the rotor flow. In this situation, the ER fluid remains in a shear banding state. Alternately, at higher frequencies (> 100 Hz), $F_\perp$ may be much smaller than F_s for all particles near either the stator or the rotator. In this case, all the ER particles have to flow. As a result, the ER fluid is located in a liquid state. Between the shear banding state and liquid state, it can be conjectured that a transition state should appear when $F_\perp$ and F_s have comparable values.

5 Discussion and Conclusions

It is worth mentioning that the present system actually contains many other forces. For example, the Brownian force, short-range repulsive forces arising from the steric interactions, adhesion forces due to water or surfactant, the van der Waals attraction, and electrostatic repulsion. In the theoretical analysis above, for simplicity, such forces have been correctly neglected since the electric interaction force produces by far the largest ER effect. In addition, to expose the basic physical mechanism, we have adopted a somewhat simplified model for calculating the electric interaction force between two ER particles, though various kinds of more complex models can be used to quantitatively improve accuracy, such as employing an energy method,[46] accounting for non-linear conduction,[47] and so on.

To sum up, we have found that as the frequency of the field is decreased, the ER fluid will go from a liquid to an intermediate transition state, and eventually to a shear banding state. Our theoretical analysis has further indicated that this phase change originates from competing effects of viscous and electrical forces.

Acknowledgments

We are grateful to Professor Kunquan Lu, Dr. Peng Tan and Mr. Wei Bao for their fruitful help and discussions, and to Dr. James Abbott for improving the English.

References

[1] T.C. Halsey, Science **258** (1992) 761.

[2] K.Q. Lu, R. Shen, X.Z. Wang, G. Sun, W.J. Wen, and J.X. Liu, Chin. Phys. **15** (2006) 2476.

[3] W.J. Wen, X.X. Huang, S. Yang, K.Q. Lu, and P. Sheng, Nature Mater. **2** (2003) 727.

[4] D. Kittipoomwong, D.J. Klingenberg, Y.M. Shkel, J.F. Morris, and J.C. Ulicny, J. Rheol. **52** (2008) 225.

[5] Z.W. Wang, Z.F. Lin, and R.B. Tao, Commun. Theor. Phys. **29** (1998) 207.

[6] R.M. Liu and J.P. Huang, Commun. Theor. Phys. **43** (2005) 765.

[7] G.Q. Zhao, S.Y. Chen, W.J. Wen, F. Miyamaru, M.W. Takeda, J.D. Yu, and P. Sheng, Soft Matter **7** (2011) 7198.

[8] M.F. Geist, K. Boussois, A. Smith, C.S. Peyratout, and D.G. Kurth, Langmuir **29** (2013) 1743.

[9] J.L. Jiang, Y. Tian, and Y.G. Meng, Langmuir **27** (2011) 5814.

[10] K.P.S. Parmar, Y. Méheust, B. Schjelderupsen, and J.O. Fossum, Langmuir **24** (2008) 1814.

[11] X.Y. Wang and V. Alvarado, J. Phys. Chem. B **113** (2009) 13811.

[12] J.G. Cao, J.P. Huang, and L.W. Zhou, J. Phys. Chem. B **110** (2006) 11635.

[13] Y. Méheust and K.P.S. Parmar, J. Rheol. **55** (2011) 809.

[14] R.C. Kanu and M.T. Shaw, J. Rheol. **42** (1998) 657.

[15] P. Calandra, G. Salvato, and F. Aliotta, ScienceJet **2** (2013) 38.

[16] J.R. Melcher and G.I. Taylor, Fluid. Mech. **1** (1969) 111.

[17] S.A. Roberts and S. Kumar, J. Fluid. Mech. **631** (2009) 255.

[18] B. Khusid and A. Acrivos, Phys. Rev. E **52** (1995) 1669.

[19] X. Tang, W.H. Li, X.J. Wang, and P.Q. Zhang, Int. J. Mod. Phys. B **13** (1999) 1806.

[20] F. Filisko and S. Henley, Int. J. Mod. Phys. B **15** (2001) 686.

[21] D.K. Liu, C. Li, J. Yao, L.W. Zhou, and J.P. Huang, Int. J. Mod. Phys. B **25** (2011) 971.

[22] D.J. Klingenberg and C.F. Zukoski, Langmuir **6** (1990) 15.

[23] O. Volkova, S. Cutillas, and G. Bossis, Phys. Rev. lett. **82** (1999) 233.

[24] J.W. Zhang, X.Q. Gong, C. Liu, W.J. Wen, and P. Sheng, Phys. Rev. Lett. **101** (2008) 194503.

[25] K.V. Pfeil, M.D. Graham, D.J. Klingenberg, and J.F. Morris, Phys. Rev. Lett. **88** (2002) 188301.

[26] C. Li, J.Y. Huang, Q.G. Tang, J.P. Huang, J.W. Zhang, and L.W. Zhou, Soft Matter **8** (2012) 5250.

[27] A. Demortière, A. Snezhko, M.V. Sapozhnikov, N. Becker, T. Proslier, and I.S. Aranson, Nat. Commun. **5** (2014) 3117.

[28] L. Xu, W.J. Tian, X.F. Wu, J.G. Cao, L.W. Zhou, J.P. Huang, and G.Q. Gu, J. Mat. Res. **23** (2008) 409.

[29] Y.C. Lan, C.K. Huang, S.Q. Men, and K.Q. Lu, Phys. Rev. E **70** (2004) 021507.

[30] Z.Y. Wang, P. Zheng, K.Q. Lu, and W.J. Wen, Appl. Phys. Lett. **82** (2003) 1796.

[31] L.C. Davis, J. Appl. Phys. **73** (1993) 680.

[32] D.L. Klass and T.W. Martinek, J. Appl. Phys. **38** (1967) 75.

[33] H. Ma, W. Wen, W.Y. Tam, and P. Sheng, Phys. Rev. Lett. **77** (1996) 2499.

[34] G. Ovarlez, S. Rodts, X. Chateau, and P. Coussot, Rheol. Acta **48** (2009) 831.

[35] A.S. Yoshimura, R.K. Prud'homme, H.M. Princen, and A.D. Kiss, J. Rheol. **31** (1987) 699.

[36] L. Onsager and S. Machlup, Phys. Rev. **91** (1953) 1505.

[37] E.J. Finnemore and J.B. Franzini, *Fluid Mechanics with Engineering Applications*, McGraw-Hill, New York (2002).

[38] J. Zheng, W.J. Fu, and L.W. Zhou, Chin. Phys. Lett. **30** (2013) 094701.

[39] P. Tan, W.J. Tian, X.F. Wu, J.Y. Huang, L.W. Zhou, and J.P. Huang, J. Phys. Chem. B **113** (2009) 9092.

[40] J.P. Huang and K.W. Yu, Phys. Rev. E **70** (2004) 061401.

[41] R. Tao and Q. Jiang, Phys. Rev. Lett. **73** (1994) 205.

[42] K.Q. Lu, W.J. Wen, C.X. Li, and S.S. Xie, Phys. Rev. E **52** (1995) 6329.

[43] J.P. Huang and K.W. Yu, Phys. Rep. **431** (2006) 87.

[44] D.A.G. Bruggeman, Ann. Phys. (Leipzig) **24** (1935) 636.

[45] J.P. Huang, K.W. Yu, and G.Q. Gu, Phys. Lett. A **300** (2002) 385.

[46] W.J. Tian, J.P. Huang, and K.W. Yu, J. Appl. Phys. **105** (2009) 102044.

[47] J.N. Foulc, P. Atten, and N. Felici, J. Electrostat. **33** (1994) 103.